STRATEGIES FOR LOW, HIGH AND HYPER VELOCITY IMPACT DAMAGE MODELLING OF STRUCTURAL COMPOSITES

L. Raimondo[1*], L. Iannucci[1], D. Pope[2], P.T. Curtis[2]

[1] *Department of Aeronautics, Imperial College London, South Kensington Campus, SW7 2AZ London, UK*

[2] *Physical Sciences Department, Building 5M, DSTL Porton Down, SP4 0JQ Salisbury, Wilts, UK*

**l.raimondo@imperial.ac.uk*

Keywords: polymer composites, impact, Finite Element Analysis (FEA).

Abstract

Challenges and recent advances in the modelling of impact damage of polymer composites for aerospace and defense applications are discussed in the present paper, including: a novel damage mechanics formulation applicable to predicting mesh-size independent impact damage in unidirectional (UD) composite laminates; a novel physics-based approach to the modelling of strain-rate-dependent elastic and failure behavior of UD composites; the application of a sub-scaling technique for ballistic impact simulations of large laminated composite targets; and a novel approach to predicting hypervelocity impact damage in high-performance fibre composites. Conclusions indicate that the proposed original solutions are valid and result in more reliable and more cost efficient impact simulations when compared to classic approaches.

1 Introduction

Advanced composite material models are increasingly being used in the design of safety-critical components and structures for aerospace or defence applications and it is crucial that predicting impact damage is as accurate as possible. However, a general lack of detailed validation of some of the strategies used within the composite community for impact damage modelling, is evident in the dedicated literature. In particular, the present authors identified certain modelling difficulties, which were encountered during almost two decades of active research in the area, and for which a satisfactory solution has not yet been made available in the literature. This paper will focus on some of these problems and summarise recent advances in the following areas: 1) mesh-size regularisation of impact results; 2) physics-based modelling of strain rate effects; 3) geometrical scaling for large scale simulations; 4) modelling of high performance fibre composites, for which characterisation of static and dynamic properties through standard testing is problematic or not at all possible.

2.1 Mesh-size objectivity in impact damage modelling.

When progressive failure is simulated with FEA by means of a Damage Mechanics (DM) approach based on a smeared crack formulation, mesh refinement results in a smaller localisation band width and thus reduces the global energy dissipated by the numerical

fracture process. A negative softening slope, adjusted as a function of a characteristic element length, and energy release rates [1], provides a simple and physically sound solution to the problem of objective energy dissipation with respect to the FE mesh size. This approach, which is commonly referred to as the "cohesive crack model", was first proposed for the numerical modelling of damage in concrete by Bazant and Oh [2]. The majority of non-linear commercial FE codes implemented the cohesive crack model. Furthermore, many researchers have applied this approach to the modelling of impact damage in advanced composite materials, e.g. [3-10]. However, despite having important implications for both the research and industrial communities, the claim that the cohesive crack model would produce mesh-size independent impact damage results has, surprisingly, never been sustained by validation. Three of the present authors recently proved that the cohesive crack model does not in fact produce mesh-size independent composite damage for generic mesh-sizes [11].
When progressive failure is simulated with FEA by means of a Damage Mechanics (DM) approach based on a smeared crack formulation, mesh-regularisation of the impact results can successfully be achieved for any mesh-size by simply scaling the energy release rates by the number of intralaminar matrix cracks in one element at cracks saturation. The number of intralaminar matrix cracks is related to the characteristic element dimensions and the intralaminar crack saturation density parameter. This is performed by making the matrix fracture energy dependent on the orientation of the fracture surface, which is predicted by the matrix failure criteria [12]:

$$\begin{cases} \left(\sigma_i^{t+\Delta t}\right) \xrightarrow{\perp x(\varphi)} \left(\sigma_{i'}^{t+\Delta t}\right) \\ \sigma_{y'}^{t+\Delta t} > 0 \rightarrow f_{mt} = \left(\dfrac{\sigma_{y'}^{t+\Delta t}}{Y_t}\right)^2 + \left(\dfrac{\tau_{x'y'}^{t+\Delta t}}{S_{xy}}\right)^2 + \left(\dfrac{\tau_{y'z'}^{t+\Delta t}}{S_{yz}}\right)^2 - 1;\ f_{mt} \geq 0 \\ \sigma_{y'}^{t+\Delta t} < 0 \rightarrow f_{mc} = \left(\dfrac{\tau_{x'y'}^{t+\Delta t}}{S_{xy} - \mu_l \sigma_{y'}^{t+\Delta t}}\right)^2 + \left(\dfrac{\tau_{y'z'}^{t+\Delta t}}{S_{yz} - \mu_t \sigma_{y'}^{t+\Delta t}}\right)^2 - 1;\ f_{mc} \geq 0 \end{cases} \quad (1)$$

where Y_t is the matrix tensile strength and S_{xy} and S_{yz} are shear strengths. The symbol $\perp x(\varphi)$ signifies a 3D rotation around the x-axis (fibre-direction axis) of an angle φ. The angle $\bar{\varphi}$, which satisfies the failure criteria for matrix tensile failure, f_{mt}, and matrix compressive failure, f_{mc}, determines the orientation of the fracture surface. The fracture surface can assume any orientation $0 \leq \bar{\varphi} \leq \pi$ depending on the loading conditions. μ_t and μ_l are transverse and longitudinal friction coefficients, respectively. When a tensile force act on the fracture surface, i.e. $\sigma_{y'} \geq 0$ and $\bar{\varphi} = 90$, the following expression is used to compute the matrix fracture energy:

$$\Gamma_m = \Gamma_I^m \left(\frac{\sigma_{y'}^{t+\Delta t | d_m^{t+\Delta t}=0}}{\sigma_m^o}\right)^2 + \Gamma_{II}^m \left(\frac{\tau_{x'y'}^{t+\Delta t | d_m^{t+\Delta t}=0}}{\sigma_m^o}\right)^2 + \Gamma_{II}^m \left(\frac{\tau_{y'z'}^{t+\Delta t | d_m^{t+\Delta t}=0}}{\sigma_m^o}\right)^2 \quad (2)$$

Where Γ_I^m is the mode I matrix fracture energy and Γ_{II}^m is the mode II matrix fracture energy, and $\sigma_m{}^0$ is the equivalent matrix failure stress [11]. On the other hand, when a compressive

force acts on the fracture surface, i.e. $\sigma_{y'} < 0$, or when a tensile force acts on the fracture surface with $\overline{\varphi} \neq 90$, the matrix fracture energy is computed as:

$$\Gamma_m = c_{num}\left[\Gamma_I^m\left(\frac{\sigma_{y'}^{t+\Delta t|d_m^{t+\Delta t}=0}}{\sigma_m^o}\right)^2 + \Gamma_{II}^m\left(\frac{\tau_{x'y'}^{t+\Delta t|d_m^{t+\Delta t}=0}}{\sigma_m^o}\right)^2 + \Gamma_{II}^m\left(\frac{\tau_{y'z'}^{t+\Delta t|d_m^{t+\Delta t}=0}}{\sigma_m^o}\right)^2\right] \tag{3}$$

The parameter c_{num} quantifies the number of intralaminar matrix cracks at saturation. This parameter can be defined as a function of the intralaminar matrix crack density at saturation parameter, c_{dens}, and element dimensions as follows:

$$c_{num} = c_{dens} L_y \tag{4}$$

In which L_y is the characteristic element length in the y-direction and l_y is defined next.

The characteristic element lengths for matrix damage modelling are defined as:

$$\begin{aligned} &\overline{\varphi} = 90^\circ \Rightarrow L_{yz} = L_z \\ &\overline{\varphi} \neq 90^\circ \Rightarrow L_{yz} = \frac{L_y}{\cos(\overline{\varphi})} \end{aligned} \tag{5}$$

By combining Equations (3), (4) and (5), the following equation is obtained:

$$\varepsilon_m^f = \frac{2c_{dens}\left[\Gamma_I^m\left(\frac{\sigma_{y'}^{t+\Delta t|d_m^{t+\Delta t}=0}}{\sigma_m^o}\right)^2 + \Gamma_{II}^m\left(\frac{\tau_{x'y'}^{t+\Delta t|d_m^{t+\Delta t}=0}}{\sigma_m^o}\right)^2 + \Gamma_{II}^m\left(\frac{\tau_{y'z'}^{t+\Delta t|d_m^{t+\Delta t}=0}}{\sigma_m^o}\right)^2\right]}{\sigma_m^o \cos(\overline{\varphi})} \tag{6}$$

i.e., when intralaminar matrix fracture energy is scaled with a number of cracks per element, the characteristic element length disappears from the computation of the ultimate failure strain: the potential damage energy increases with increasing FE volume. It could be speculated that the topological information, which is provided by the characteristic length in the cohesive crack model, and which is required for mesh-size-regularisation, is not absent in the modified cohesive crack formulation proposed in Equation (6). The crack density parameter, which replaces the characteristic length which would have appeared at the denominator of Equation (6), e.g. [2], has also units of mm^{-1}.

Figure 1 shows a comparison of experimental and numerical results. These were obtained for two different target discretisation strategies, i.e. FE's with in-plane dimensions of $1mm^2$ and $2mm^2$ (in both cases 0.34mm thick) respectively, and two different mesh-regularisation approaches, i.e. the classic cohesive crack model and the modified approach, which were both

implemented. The value $c_{dens} = 5.25mm^{-1}$ was used for the case labelled as "2mm Mesh – Proposed model".

The results presented in Figure 1 show that mesh-size independent impact damage analysis can be successfully achieved with the proposed method for any target discretisation strategy. These results also show that the classic implementation of the cohesive crack model is invalid for mesh-regularisation of the impact results for a mesh-size that exceeds the distance between two adjacent cracks. Because this distance may be system dependent, and it may be difficult to characterise for impact loading conditions, a crack density parameter should always be used for impact damage modelling with a smeared crack (energy based) formulation, regardless of the mesh-size.

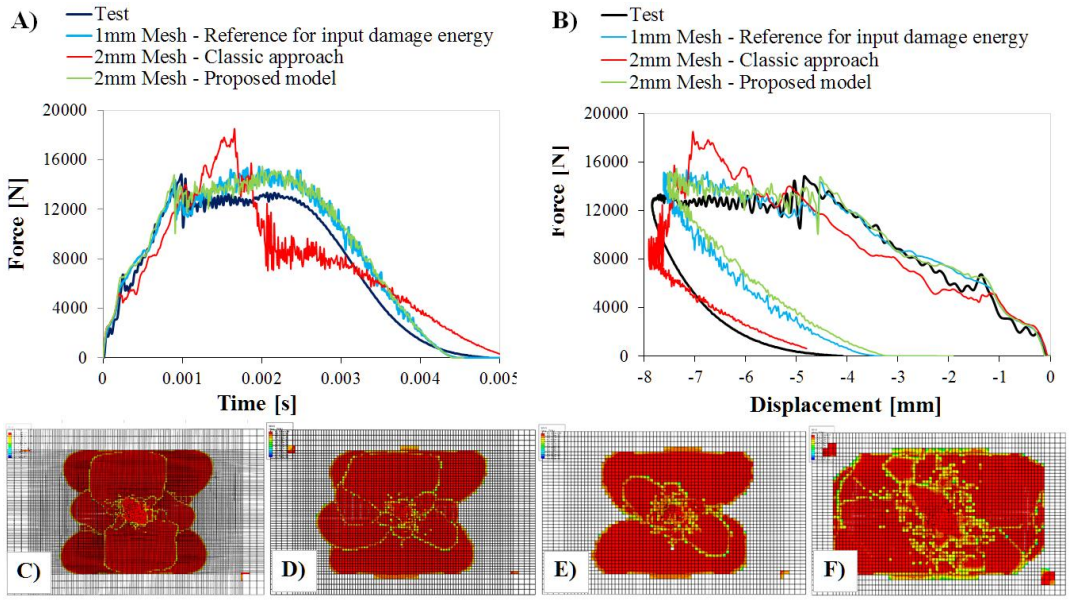

Figure 1. Numerical and experimental impact results for a QI target discretized with two different mesh-densities, and impacted at 75J impact energy. A) Force-time histories; B) Force-displacement plots; Envelope of the matrix damage variable: C) 1mm^2 FE size; D) 1.5mm^2 FE size; E) 2mm^2 FE size using the proposed model; F) 2mm^2 FE size using the cohesive crack model.

2.2 Phenomenological based modelling of strain rate effects.

Macro-mechanically based models have been developed to predict the 3D non-linear behaviour of polymer composites and these are founded on classic plasticity theories. One of the advantages of the models based on plasticity theories is that they can be easily extended for predicting strain rate effects, and can be implemented in FE for numerical analysis, e.g. [13-15]. These models typically require that parameters are defined from fitting of data from a full range of off-axis tests for predicting the composite's behaviour in the generic case. The applicability of classic visco-plastic models, when the 3D plastic potential is not characterised, is in fact limited to uni-axial loading conditions [14]. Visco-plasticity combined with micro-mechanics approaches have also been proposed, e.g. [16-17]. These require that constituent elastic constants are determined from composite data using micromechanics, which is a limitation because it requires further computational effort. Dynamic failure theories have also been proposed for UD composites, but they typically require high-rate tests data to be produced for many different specimen configurations [18]. However, three of the current authors have recently shown [19] that the off-axis dynamic behaviour of UD carbon fibre polymer composites can be fully predicted, i.e. moduli and strength, when data is produced

from a very limited number of Quasi-Static (QS) and dynamic tests for only one specimen configuration. This is a dramatic improvement compared to what is required for applicability of other currently available modelling techniques. This newly developed theory is very suitable for application in impact damage analysis, as it is phenomenological-based and the loading conditions created in the target upon impact are likely to exceed the space of characterisation achievable through standard high-rate testing. The key assumption in the theory is that, for carbon fibre polymer composites, the only mode of deformation that is strain rate sensitive is the matrix shear mode, and that strain rate effects on both strength and stiffness in modes other than shear are a 3D effect, due to the fact that the planes of maximum shear stress are at an angle to the principal planes of material symmetry. Following on this hypothesis phenomenological failure criteria can be defined for dynamic loading conditions as follows [19]:

$$f_{fc} = \frac{\sigma_x}{k\left(\dot{\varepsilon}_x^t\right)X_c^{qs}} + \frac{\tau_{xy}}{k\left(\dot{\gamma}_{xy}\right)S_{xy}^{qs}} + \frac{\tau_{zx}}{k\left(\dot{\gamma}_{zx}\right)S_{zx}^{qs}} - 1 \geq 0 \tag{7}$$

$$f_{fc} = \frac{\sigma_x}{X_c^{qs}} + \left(\frac{\tau_{xy}}{k\left(\dot{\gamma}_{xy}\right)S_{xy}^{qs}}\right)^{\alpha} + \left(\frac{\tau_{zx}}{k\left(\dot{\gamma}_{zx}\right)S_{zx}^{qs}}\right)^{\alpha} - 1 \geq 0 \tag{8}$$

$$f_{mt} = \left(\frac{\sigma_{y'}}{Y_t^{qs}}\right)^2 + \left(\frac{\tau_{xy'}}{k\left(\dot{\gamma}_{xy'}\right)S_{xy}^{qs}}\right)^2 + \left(\frac{\tau_{y'z'}}{k\left(\dot{\gamma}_{y'z'}\right)S_{yz}^{qs}}\right)^2 - 1 \geq 0 \tag{9}$$

$$f_{mc} = \left(\frac{\tau_{xy'}}{k\left(\dot{\gamma}_{xy'}\right)S_{xy}^{qs} - \mu_l^d\sigma_{y'}}\right)^2 + \left(\frac{\tau_{y'z'}}{k\left(\dot{\gamma}_{y'z'}\right)S_{yz}^{qs} - \mu_t^d\sigma_{y'}}\right)^2 - 1 \geq 0 \tag{10}$$

Where the same high-rate scaling function, $k\left(\dot{\varepsilon}_i\right)$, is used for all strength parameters. The scaling function is characterised with QS and dynamic experimental strength data for one only mode of deformation, and can be defined from a polynomial fit of the normalised in-plane shear strength versus shear strain rate values:

$$k\left(\dot{\gamma}_{xy}\right) = K_0 + K_1 \log_{10}\dot{\gamma}_{xy} + K_2 \log_{10}^2\dot{\gamma}_{xy} \tag{11}$$

Strain rate affects “progressive failure”, i.e. plastic flow and matrix cracking in polymers and polymer composites. A distinction is made between the physical concept of “fracture surface”, which has originally been used in [20], and the physical concept of “surface of progressive failure”, which we introduced to simulate resistance to progressive failure observed in composites subjected to higher rate loading conditions.
The “potential fracture surface” can be used to define the orientation of this plane, on which progressive failure, i.e. visco-plasticity effects when the focus is on strain rate effects, accumulates in a composite volume under generic loading conditions.
This orientation, i.e. $\overline{\varphi}$, is defined as the maximum of the functional part of the matrix compressive failure criterion, Equation (10):

$$\begin{cases} f_{mc}^{t+\Delta t}(\varphi)=\left(\dfrac{\tau_{xy'}^{t+\Delta t}(\varphi)}{k\left(\dot{\gamma}_{xy'}(\varphi)\right)S_{xy}^{qs}-\mu_l^{qs}\sigma_{y'}^{t+\Delta t}(\varphi)}\right)^2+\left(\dfrac{\tau_{y'z'}^{t+\Delta t}(\varphi)}{k\left(\dot{\gamma}_{y'z'}(\varphi)\right)S_{yz}^{qs}-\mu_t^{qs}\sigma_{y'}^{t+\Delta t}(\varphi)}\right)^2 \\ \overline{\varphi}: f_{mc}^{t+\Delta t}(\overline{\varphi})> f_{mc}^{t+\Delta t}(\varphi)\forall\,\varphi\in[0,2\pi[\end{cases} \quad (12)$$

Strain-rate induced hardening are thus predicted by modelling strain rate dependent shear stress-strain response on the "progressive failure plane", whose orientation is predicted by the above Equation (12), through the stress update procedure:

$$\begin{bmatrix}\Delta\varepsilon_x^{t+\Delta t}\\ \Delta\varepsilon_y^{t+\Delta t}\\ \Delta\varepsilon_z^{t+\Delta t}\\ \Delta\gamma_{xy}^{t+\Delta t}\\ \Delta\gamma_{yz}^{t+\Delta t}\\ \Delta\gamma_{zx}^{t+\Delta t}\end{bmatrix}\xrightarrow{\perp x(\overline{\varphi})}\begin{bmatrix}\Delta\varepsilon_x^{t+\Delta t}\\ \Delta\varepsilon_{y'}^{t+\Delta t}\\ \Delta\varepsilon_{z'}^{t+\Delta t}\\ \Delta\gamma_{xy'}^{t+\Delta t}\\ \Delta\gamma_{y'z'}^{t+\Delta t}\\ \Delta\gamma_{z'x}^{t+\Delta t}\end{bmatrix}\Rightarrow\begin{Bmatrix}k\left(\dot{\varepsilon}_x^{t+\Delta t}\right)\\ k\left(\dot{\gamma}_{xy'}^{t+\Delta t}\right)\\ k\left(\dot{\gamma}_{y'z'}^{t+\Delta t}\right)\\ k\left(\dot{\gamma}_{z'x}^{t+\Delta t}\right)\end{Bmatrix}$$

$$\begin{bmatrix}\Delta\sigma_x^{t+\Delta t}\\ \Delta\sigma_y^{t+\Delta t}\\ \Delta\sigma_z^{t+\Delta t}\\ \Delta\tau_{xy}^{t+\Delta t}\\ \Delta\tau_{yz}^{t+\Delta t}\\ \Delta\tau_{zx}^{t+\Delta t}\end{bmatrix}\xrightarrow{\perp x(\overline{\varphi})}\begin{bmatrix}\Delta\sigma_x^{t+\Delta t}\\ \Delta\sigma_{y'}^{t+\Delta t}\\ \Delta\sigma_{z'}^{t+\Delta t}\\ \Delta\tau_{xy'}^{t+\Delta t}\\ \Delta\tau_{y'z'}^{t+\Delta t}\\ \Delta\tau_{z'x}^{t+\Delta t}\end{bmatrix}\Rightarrow\begin{bmatrix}\Delta\sigma_x^{t+\Delta t}\\ \Delta\sigma_{y'}^{t+\Delta t}\\ \Delta\sigma_{z'}^{t+\Delta t}\\ k\left(\dot{\gamma}_{xy'}^{t+\Delta t}\right)\Delta\tau_{xy'}^{t+\Delta t}\\ k\left(\dot{\gamma}_{y'z'}^{t+\Delta t}\right)\Delta\tau_{y'z'}^{t+\Delta t}\\ k\left(\dot{\gamma}_{z'x}^{t+\Delta t}\right)\Delta\tau_{z'x}^{t+\Delta t}\end{bmatrix}\xrightarrow{\perp x(-\overline{\varphi})}\begin{bmatrix}\Delta\sigma_x^{t+\Delta t}\\ \Delta\sigma_y^{t+\Delta t}\\ \Delta\sigma_z^{t+\Delta t}\\ \Delta\tau_{xy}^{t+\Delta t}\\ \Delta\tau_{yz}^{t+\Delta t}\\ \Delta\tau_{zx}^{t+\Delta t}\end{bmatrix}^{dyn} \quad (13)$$

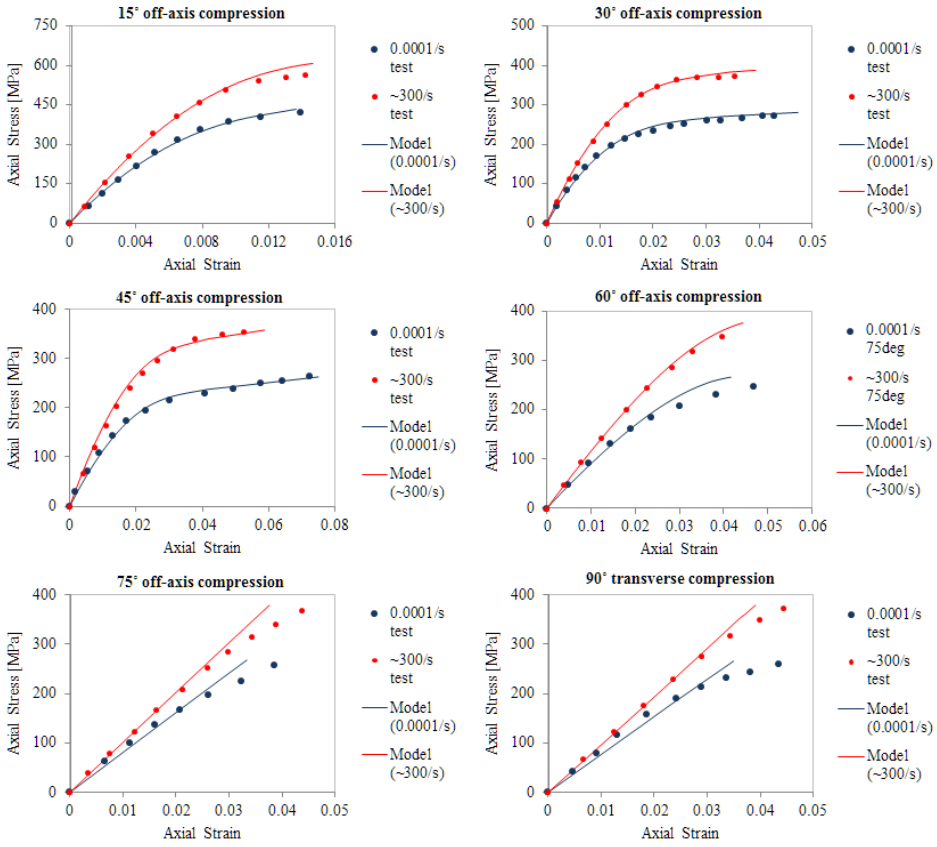

Figure 2. Numerical and experimental [21] QS and dynamic off-axis compressive behaviour of an IM7-8552 UD composite.

Results from one-solid element numerical simulations of the compressive QS and dynamic off-axis behaviours are presented in Figure 2 using experimental results from [21]. The numerical results are truncated at the predicted value of failure stress, which shows that the proposed dynamic failure criteria can predict strength values for all off-axis cases in excellent agreement with the experimental results, for both QS and dynamic loading conditions. Strain rate induced material hardening effects are also excellently captured at the higher loading rate. The moduli are predicted very accurately for all dynamic cases. This validates the use of a same strain rate dependent scaling function for both strength and moduli, on the potential surface for progressive failure, at least for the IM7-8552 UD composite material which was investigated.

3 Bringing it all together: reducing computational cost for large scale structural simulations.

The strategies described in 2.1 and 2.2 were implemented in ABAQUS/Explicit in a 3DVUMAT applicable to predicting the high velocity impact behavior of relatively large (0.5 m^2) and thick (up to 18 mm) composite panels for use in an industrial virtual test campaign for design against hard debris impact.

For application of the 3DVUMAT it is necessary that a minimum of one element per ply through-thickness of the composite target is used for its discretization. When considering that the thicker panels had 72 plies through-thickness, a total of approximately 253 million 3D solid elements (C3D8R) would be required for discretization of such panels with a structured mesh of aspect ratio of 1. 253 million C3D8R elements correspond to a total of over 6 billion degrees of freedom (DOF). It is evident that conducting a virtual test campaign using such a discretization approach is unfeasible even when an advanced high performance cluster is available. The number of DOF could be reduced by using elements with aspect ratio greater than 1. However, a more dramatic reduction of the number of DOF was achieved by using the shell-to-solid coupling feature, which is available in the commercial version of ABAQUS/Explicit. From analysis of the published literature, this feature does not seem to have been applied before to high velocity impact studies.

All panels were modeled using both 3D and 2D finite elements with large aspect ratio, and the shell-to-solid coupling option was used to couple the regions containing the 3D and 2D finite elements. The contact region of the target, with a size of 100mm x 100mm in-plane dimensions, and the cubic impactor, were modeled using C3D8R solid elements, and the rest of the target was modeled using 2D shell elements.

The 3D elements mesh size was fixed, and elements with dimensions of 1 mm x 1 mm x 0.25 mm (0.25 mm was equal to the ply thickness) were used for the target at the impact point. Large 10mm x 10mm - with variable thickness - shell elements were used for discretizing the outer region of the panels. To illustrate the advantages of using the shell-to-solid coupling option, the case of an 18 mm thick panel is taken as an example. For this panel, the number of DOF was reduced from 380 million to 17 million, i.e. a 20 folds reduction factor. Despite it is difficult to estimate the CPU times accurately due to the massive scale of the problem, it is possible to estimate that the CPU time could be reduced of a factor several times greater than 20. In fact, explicit solution times typically increase non-linearly with increasing number of elements in the model.

The size of the numerical problem required the adoption of important simplifications in the approach to modeling, such as the use of a smeared formulation and sub-scaling. Focus was put on developing a strategy for predicting residual velocities for various panel thicknesses and lay-ups. An industry capable approach was thus designed to meet this requirement. A series of steps were identified, and are summarized here. Industry need to:

1) Obtain ballistic results for a series of high velocity impact tests on small (and thin) composite targets, preferably at impact velocities much higher than the ballistic limit. The data should include weight of the target before and after impact.
2) Perform numerical simulations of the tests described in step 1) and determine the value of the required erosion parameter [5] with an inverse approach (size of the 3D elements should be fixed at this scale).
3) Perform the full scale simulations using the value of the penetration parameter and the same mesh size, derived and used in step 2).

Preliminary simulations showed that the shell-to-solid coupling constraint could not be used for failure and damage modeling of the coupling region at the higher impacts energies. The coupling region failed, and so the shell-to-solid constraints when the elements softened (failed) in this region, see Figure 3.

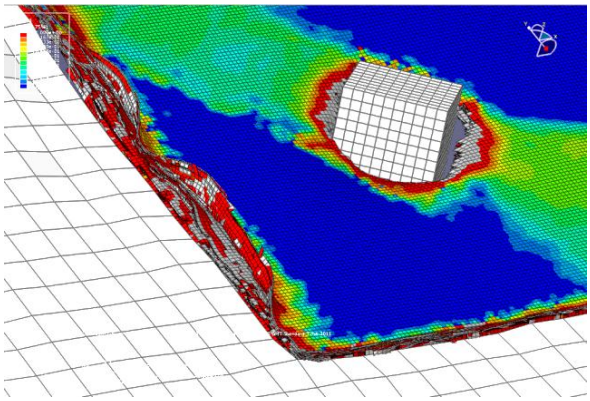

Figure 3. View of a damaged 6mm thick target. The fringe plot is for matrix damage. Failure of the elements at the shell-to-solid coupling boundary results in failure of the shell-to-solid coupling constraint.

A solution to this problem was achieved by defining purely elastic boundaries in the 3D portion of the model at the shell-to-solid coupled region. This was done by partitioning the 3D parts with subsequent definition of two sections. The partition of the front layer of the solid portion of the target is illustrated in Figure 4 (left). The outer region of the 3D parts was assigned a different section definition compared to the inner region. An additional set of VUMAT input parameters was assigned to the section at the boundaries of the 3D-2D solid-shell domain, that had very high UD ply strength values (~10^9MPa) but all other UD ply properties identical to the UD ply material properties.
Figure 4 (right) shows the simulation of an 18 mm thick panel. In this figure the fringe plots were for matrix damage.
Figure 5 shows a comparison between a HSDC still and an image from the numerical simulations at the same impact time for the back face of a 6mm UERF panel. The blue arrows point at the border of the flexural waves in the experimental panel and in the model. It is evident that the flexural wave expanded qualitatively alike and with the same speed in the model as in the test panel.
Finally, Figure 6 shows the comparison between the experimental data for 4 different panel thicknesses and the numerical results from 12 simulations. In this Figure 6, the triangular markers indicate the experimental data points, and the square markers indicate the numerical data points. The trend lines are a linear fit to the experimental data. An excellent correlation was obtained between predicted and experimental data points in the residual velocity vs. impact velocity plane with the proposed methodology.

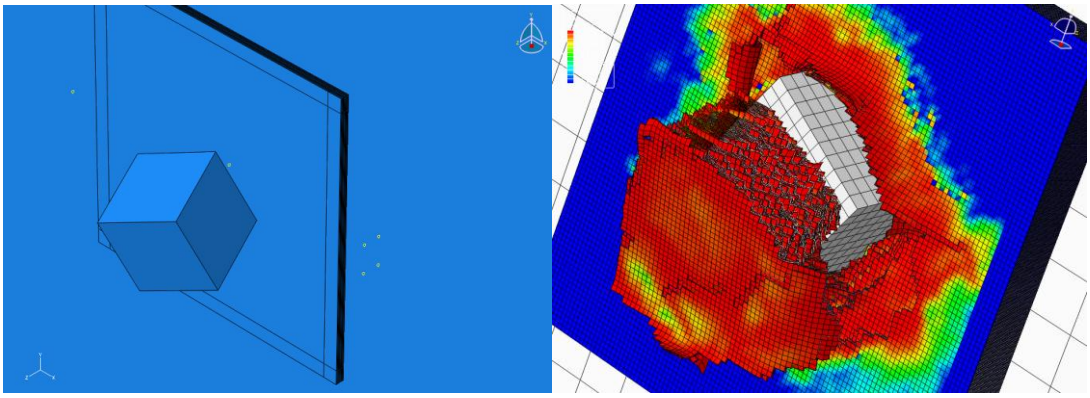

Figure 4. (left) Detail of the assembly that shows the cube, the central 3D solid mesh and the outer 2D mesh. Partition of the first solid 3D part is visible in the figure; (right) successful shell-to-solid coupling constraint for a damaging 18mm thick panel, impacted at 218m/s by a 176g steel cube. The fringe plot is for matrix damage. Note the elastic region at the shell-to-solid boundary.

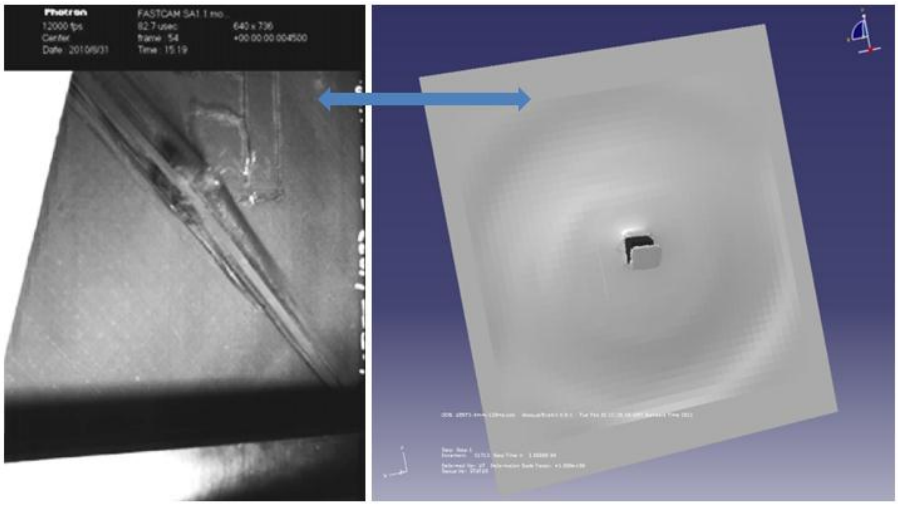

Figure 5. Comparison between still image extracted from a HSDC video and numerical simulation at 300 μs impact time. Back face of a 6mm thick target impacted at 164m/s.

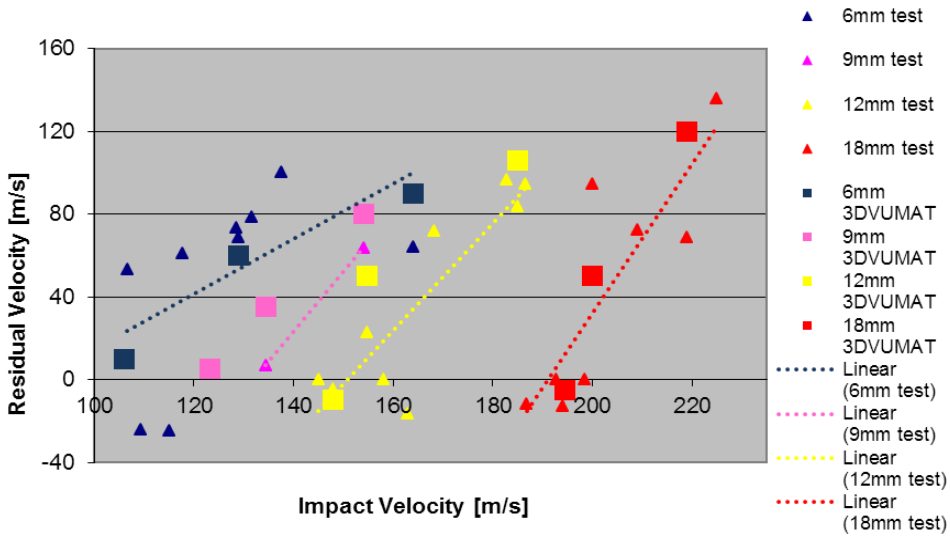

Figure 6. Comparison between experimental and numerical data points from ballistic tests and simulations of the panels for different target thicknesses.

4 The modelling of the hyper velocity behavior of high performance fibre composites: when not all material input properties are available.

One of the major challenges when simulating high performance fibre composites, e.g. Dyneema, is that not all relevant material input properties can be characterized using standard testing techniques. This is because these composites show strongly anisotropic failure properties, which is due mainly, but not only, to high fibre volume content. For instance, typical volume fractions reach as high as 85% for Dyneema laminates used in defense applications, thus testing of some of their properties yields to failure in modes other than those for which the tests are being carried out. A successful modelling strategy for 2D simulations of high velocity impacts onto thin Dyneema targets was proposed by two of the current authors [22]. For hyper velocity impact simulations, i.e. for impact velocities at around and beyond 1 km/s, and for thicker targets, a 3D formulation becomes a requirement due to the need for modelling shock (compressibility) effects, as well as for the need to include delamination modelling.

The formulation proposed in [22] was extended to 3D and coupled with a Mie-Gruneisen Equation of State (EOS) and implemented as a UMAT in DYNA3D. The targets were modeled using several layers of solid elements in cohesive contact, mix-mode delamination capable, which is a contact option available in the commercial version of DYNA3D. The aim of the research was to predict the ballistic limit of thick Dyneema targets at impact velocities beyond 1 km/s. The back face deflection time history was characterized experimentally using high speed cameras as the displacement time-history of a point in the center of the back face of the impacted panels.

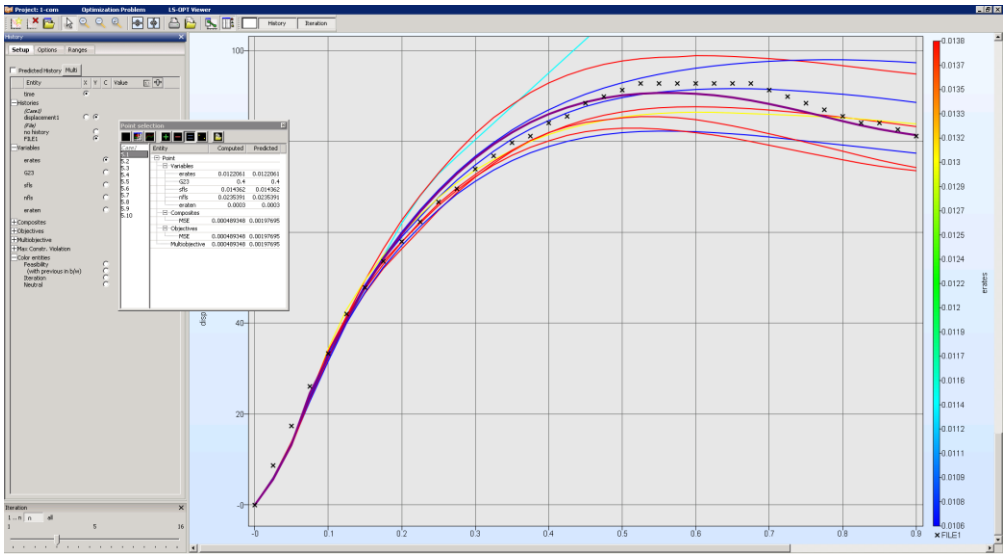

Figure 7. Experimental (dotted) and numerical (solid) back face deflection time-histories for a 40mm thick Dyneema panel impacted at 1km/s. The different curves are from different runs during a same LS-OPT optimisation analysis.

Because of the lack of the full range of material properties, excellent agreement between numerical and experimental results for hyper velocity impact against could only be obtained using a two steps approach: 1) preliminary optimisation analyses were conducted using LS-OPT coupled with DYNA3D for a case below the ballistic limit (BL) of the target. In this part of the work, the values of the unknown properties were down-selected by LS-OPT from History Mean Squared Error (MSE) based comparison of the experimental and numerical deflection time-histories, see Figure 7, which shows the result from Iteration 5 of the LS-OPT optmisation run; 2) simulations using the properties derived during step 1) were performed for

both cases above and below the BL of the target. The predicted back face deflection time-histories from step 2) are shown in Figure 8.
Figure 9 and 10 show that excellent qualitative agreement was also obtained between the deformed and damaged shapes of the numerical and experimental panels.

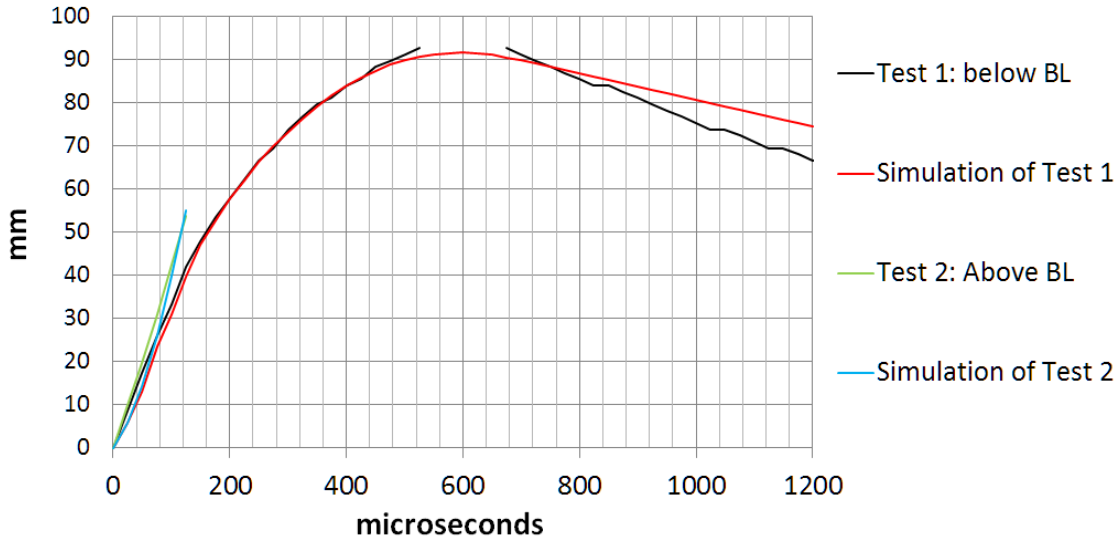

Figure 8. Experimental and numerical back face deflection time-histories for a 40mm thick Dyneema panel impacted below and above its ballistic limit using optimised input properties.

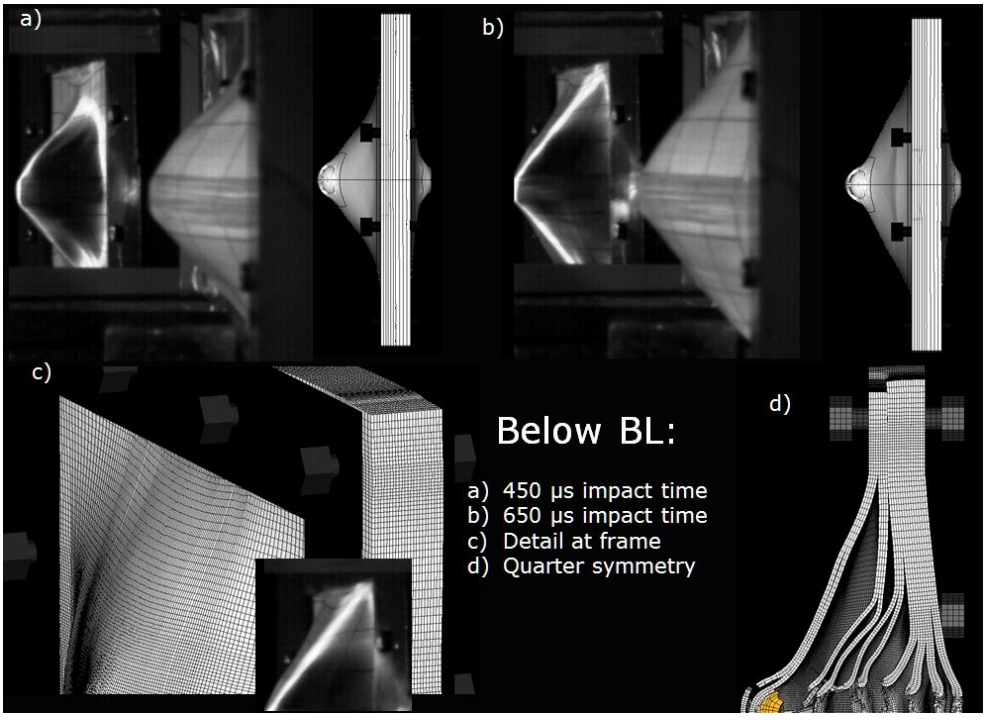

Figure 9. Comparison between experimental High Speed Digital Camera stills and numerical results for a hyper-velocity impact (below BL) of a 40mm thick Dyneema composite panel.

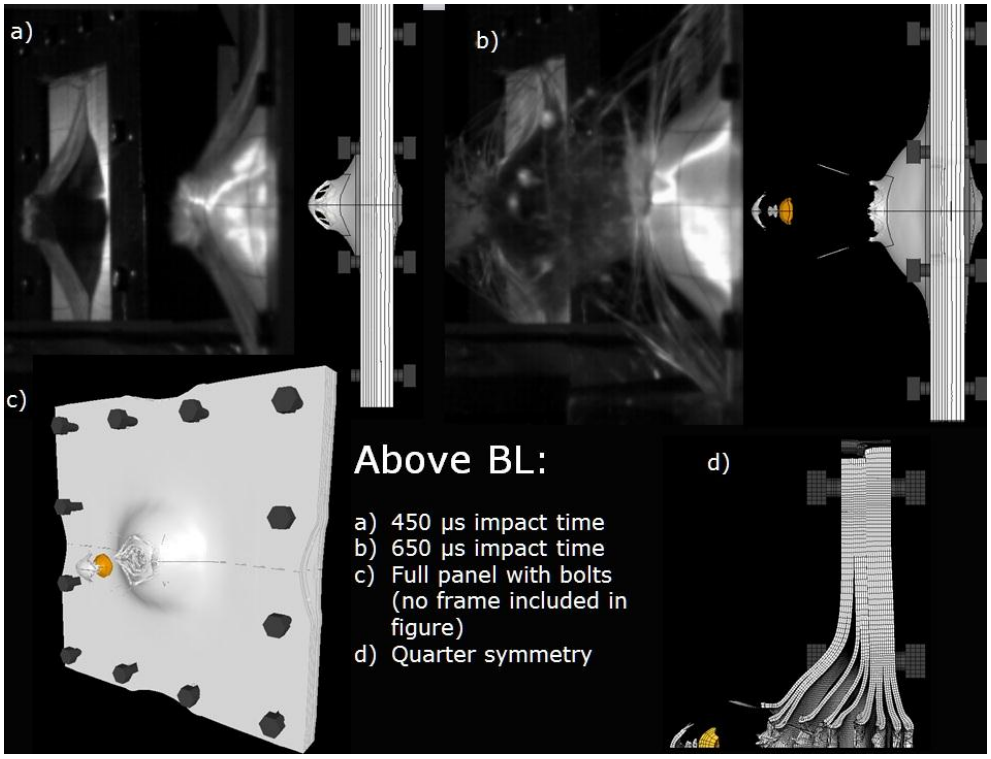

Figure 10. Comparison between experimental High Speed Digital Camera stills and numerical results for a hyper-velocity impact (above BL) of a 40mm thick Dyneema composite panel.

Conclusions

This paper has presented recent advances in the areas of low, high and hyper-velocity impact modelling of structural composites with FE and in-house developed constitutive formulations.
The development of a solution for mesh-size objective impact results, which is valid for the generic mesh-size, is of particular importance for the research and industrial communities interested in virtual, low-velocity impact testing of composites. Intralaminar matrix damage can be extensive in composite targets impacted at higher energies, thus it is necessary to use a correct matrix crack density for mesh-size regularization especially when the targets are discretized with relatively coarse meshes.
For high velocity impact modelling, i.e. when target penetration is a concern, energy dissipation is mainly driven by fibre fracture energy, thus the use of a rigorous mesh-size regularization approach for matrix damage energy may only have a second order effect on the predicted ballistic limit. However, high velocity impacts are stress-waves dominated events, and thus it is important to allow for the correct matrix damage energy to be dissipated and for strain-rate effects to be modeled accurately on elasticity and strength of the target. The proposed new strain-rate dependent elastic and failure theory described in this paper is especially suitable for high-velocity impact modelling, as it is physics-based and thus it can be more confidently applied to impact analysis than curve-fitting based dynamic failure theories. In fact, during penetrating impacts, the loading space is likely to exceed the space of characterization of the fitting coefficients. Also, the newly proposed theory has the evident advantage of requiring calibration of only one parameter through only one series of tests. Other strain-rate dependent theories typically require many more tests for calibration.
A good constitutive formulation is not always sufficient to efficiently modelling impact against composite targets. If the scale of the problem is too large for instance, computational cost may prohibit a virtual test campaign that requires explicit analysis. This is a problem for the aerospace and defense industries, where full scale simulations are rapidly replacing full scale testing. The third part of this paper described a solution for the high-velocity impact

modelling of large targets. The use of a sub-scaling approach, based on applying a shell-to-solid coupling technique for discretization of the target, i.e. solid elements were used only where they were strictly needed at the contact region, showed very successful at dramatically reducing otherwise prohibitively large computational costs.
Another problem that was discussed in this paper is the modelling of composite targets when not all input material properties required by the model can be experimentally characterized. This is typically the case when modelling high performance fibre composites. The last part of the paper showed that preliminary impact tests results can be confidently used for calibration of the missing input properties. Commercially available optimization software was used for this purpose. It was shown that determination of the missing properties through optimization, and using impact results, allow prediction of the BL of a Dyneema target impacted at velocities beyond 1 Km/s with remarkable qualitative and quantitative agreement with the experimental tests results.

Acknowledgements
The authors would like to gratefully acknowledge the funding from the Engineering and Physical Sciences Research Council (EPSRC) and the Defence Science and Technology Laboratory (DSLT) for this research under the project "Improving Survivability of Structures to Impact and Blast Loadings" EP/G042861/1.

References
[1] Hillerborg A., Modeer P.E., Peterson P.E. Analysis of crack formation and crack growth in concrete by means of F. M. and finite elements. *Cement Concrete Res*, **Volume 6**, pp. 773-782 (1976)
[2] Bazant Z.P., Oh B.H. Crack band theory for fracture of concrete. *Mater Struct*, **Volume 16**, pp. 155-77 (1983).
[3] Iannucci L., Ankersen J. An energy based damage model for thin laminated composites. *Comp Sci Tech*, **Volume 66**, pp. 934-951 (2006).
[4] Iannucci L., Willows M.L. An energy based damage mechanics approach to modelling impact onto woven composite materials. Part I: Numerical models. *Compos Part A-Appl S*, **Volume 37**, pp. 2041-2056 (2006).
[5] Raimondo L., Iannucci L., Robinson P., Pinho S.T. A numerical material model for predicting the high velocity impact behaviour of polymer composites. *Computational Methods in Applied Sciences*, **Volume 10**, pp. 161-77 (2008).
[6] Donadon M.V., Iannucci L., Falzon B.G., Hodgkinson J.M., de Almeida S.F.M. A progressive failure model for composite laminates subjected to low velocity impact damage. *Comput Struct*, **Volume 86**, pp. 1232-52 (2008).
[7] Faggiani A., Falzon B.G. Predicting low-velocity impact damage on a stiffened composite panel. *Compos Part A-Appl S*, **Volume 41**, pp. 737-49 (2010).
[8] Lopes C.S., Camanho P.P., Gurdal Z., Maimi' P., Gonzalez E.V. Low-velocity impact damage on dispersed stacking sequence laminates. Part II: Numerical simulations. *Compos Sci Technol*, **Volume 69**, pp. 937-47 (2009).
[9] Clegg R.A., White D.M., Riedel W., Harwick W. Hypervelocity impact damage prediction in composites: Part I—material model and characterisation. *Int J Impact Eng*, **Volume 33**, pp. 190-200 (2006).
[10] Yokoyama N.O., Donadon M.V., de Almeida S.F.M. A numerical study on the impact resistance of composite shells using an energy based failure model. *Compos Struct*, **Volume 93**, pp. 142-52 (2010).

[11] Raimondo L., Iannucci L., Robinson P., Curtis P.T. A progressive failure model for mesh-size-independent FE analysis of composite laminates subject to low-velocity impact damage. *Compos Sci Technol*, **Volume 72**, pp. 624-32 (2012).
[12] Pinho S.T., Iannucci L., Robinson P. Physically-based failure models and criteria for laminated fibre-reinforced composites with emphasis on fibre kinking: Part I: Development. *Comp Part A*, **Volume 37**, pp. 63-73 (2006).
[13] Weeks C.A., Sun C.T. Modeling non-linear rate-dependent behavior in fiber-reinforced composites. *Compos Sci Technol*, **Volume 58**, pp. 603-11 (1998).
[14] Thiruppukuzhi S.V., Sun C.T. Models for the strain rate dependent behaviour of polymer composites. *Compos Sci Technol*, **Volume 61**, pp. 1-12 (2001).
[15] Espinosa H.D., Lu H.C., Zavattieri P.D., Dwivedi S. A 3-D Finite Deformation Anisotropic Visco-Plasticity Model for Fiber Composites. *J Compos Mat*, **Volume 35**, pp. 369-410 (2001).
[16] Goldberg R.K., Stouffer D.C. Strain Rate Dependent Analysis of a Polymer Matrix Composite Utilizing a Micromechanics Approach. *J Compos Mater*, **Volume 36**, pp. 773-94 (2002).
[17] Tabiei A., Aminjikarai S.B. A strain-rate dependent micro-mechanical model with progressive post-failure behavior for predicting impact response of unidirectional composite laminates. *Compos Struct*, **Volume 88**, pp. 65-82 (2009).
[18] Daniel I.M., Werner B.T., Fenner J.S. Strain-rate-dependent failure criteria for composites. *Compos Sci Technol*, **Volume 71**, pp. 357-364 (2010).
[19] Raimondo L., Iannucci L., Robinson P., Curtis P.T. Modelling of strain rate effects on matrix dominated elastic and failure properties of unidirectional fibre-reinforced polymer–matrix composites. *Compos Sci Technol*, **Volume 72**, pp. 819-27 (2012).
[20] Puck A. Festigkeitsanalyse von Faser-Matrix-Laminaten. Munich, Hanser (1996).
[21] Koerber H., Xavier J., Camanho P.P. High strain rate characterisation of unidirectional carbon-epoxy IM7-8552 in transverse compression and in-plane shear using digital image correlation. *Mech Mat*, **Volume 42**, pp. 1004-19 (2010).
[22] Iannucci L., Pope D. High velocity impact and armour design. *eXPRESS Polymer Letters*, **Volume 5**, pp. 262-72 (2011).